GAMOW–TELLER TRANSITIONS AND β-DECAY PROPERTIES OF ^{74}Kr: EFFECTS OF DEFORMATION AND RESIDUAL INTERACTIONS

Sadiye Meral Cakmak

Program of Medical Monitoring Techniques, Osmangazi University, Turkey

Received 3 October 2025, accepted 24 February 2026, published online 9 March 2026

Gamow–Teller (GT) transitions play a fundamental role in exploring nuclear structure and weak-interaction-mediated decay modes. In this study, a detailed investigation of the GT strength distributions for the neutron-deficient nucleus ^{74}Kr is presented. The theoretical framework is based on the Quasiparticle Random Phase Approximation (QRPA), incorporating both particle–hole (*ph*) and particle–particle (*pp*) residual interactions. To examine the influence of different interactions, comparative analyses are performed using a schematic model and the Pyatov method. The resulting GT strength distributions are systematically compared with available experimental data to evaluate the predictive capacity of the employed models. This work contributes to a deeper understanding of spin–isospin excitations in nuclei near the $N \approx Z$ line and provides valuable insights for future studies on weak-interaction processes in exotic nuclei.

DOI:10.5506/APhysPolB.57.3-A2

1. Introduction

Weak nuclear interactions, particularly β-decay and electron capture, are deeply connected to the behavior of spin–isospin excitations in nuclei. Among these, Gamow–Teller (GT) transitions are of great significance due to their sensitivity to nuclear structure and their crucial role in nucleosynthesis pathways in astrophysical environments such as supernovae and X-ray bursts. The β-decay GT strength distributions, particularly from low-lying excited 0^+ states, are key to characterizing so-called waiting-point nuclides that slow down the r-process path due to their relatively long lifetimes [1]. In high-temperature scenarios, the thermal population of these states significantly alters the effective lifetime of the parent nucleus.

The $A \sim 70$ region near the proton-drip line presents additional complexity due to shape coexistence and mixing phenomena, which play a decisive role in shaping the nuclear configurations of even–even and odd–odd isotopes [2]. Minor variations in nucleon number can cause abrupt structural changes. Moreover, nuclei close to the $N = Z$ line experience competing pairing correlations between nucleons and between neutrons and protons which profoundly influence their decay properties [3–5].

The r-process, responsible for forming heavy neutron-rich nuclei beyond iron, relies on accurate theoretical predictions of β-decay half-lives and β-delayed neutron emission probabilities, particularly for nuclei far from stability [6]. These predictions are not only essential for astrophysical models but also for advancing our understanding of the interplay between nuclear structure and decay dynamics. In the β-decay theory, a reliable description of the parent nucleus's ground state and the excitation spectrum of the daughter nucleus is essential to predict the GT strength distribution. Any significant discrepancy points to inadequacies in the underlying theoretical formalism [7].

The difficulty of directly solving the many-body Schrödinger equation has led to the development of several approximate models. One such model, the QRPA, builds upon the RPA formalism by incorporating pairing interactions through Bogoliubov's method. In this formalism, both particle–hole (ph) and particle–particle (pp) interactions are incorporated, allowing for more accurate predictions for open-shell and mid-mass nuclei [8, 9]. The QRPA approach has been enriched by incorporating deformation effects using the Nilsson orbitals, Woods–Saxon potentials, and residual separable interactions within the Hartree–Fock–BCS framework [10–13].

In this context, the Pyatov method provides a systematic way of restoring broken symmetries in the effective Hamiltonian, especially in problems involving GT, isobaric analog (IAR), or magnetic dipole (MDR) transitions [14]. Within this method, effective interaction terms are adjusted to satisfy commutation relations between the distorted GT operator and the Hamiltonian [15]. It has been successfully applied to a variety of nuclear structure problems, including scissors modes in deformed nuclei [16], isospin mixing in odd-mass nuclei [17], and GT transitions in spherical and deformed systems [18–20].

The nuclear structure of ^{74}Kr has been extensively studied both experimentally and theoretically due to its pronounced shape coexistence and sensitivity to configuration mixing. Experimental studies at CERN/ISOLDE using total absorption spectroscopy revealed GT strength fragmentation in the Q_{EC} window and evidence of shape mixing in the ground state [21]. Measurements of electric monopole (E_0) transitions between 0^+ states further support this interpretation [4, 22–24].

A comprehensive theoretical investigation of the Gamow–Teller (GT) strength distributions in the neutron-deficient nucleus ^{74}Kr is performed within the QRPA framework in this study. The Schematic Model (SM) is applied to both spherical and deformed configurations, whereas the Pyatov Method (PM) is employed only for the spherical case to calculate the $\log(ft)$ values and B(GT) strengths. The sensitivity of the results to the particle–hole (ph) and particle–particle (pp) interaction channels is explored, and the impact of deformation on the transition strength distributions is examined. The calculated half-lives and GT strengths are presented and compared with available experimental data to assess the performance of the adopted models. This work provides further insights into weak-interaction processes in $N \approx Z$ nuclei and contributes to the broader understanding of nuclear-structure evolution near the proton-drip line. In the following sections, the theoretical framework is presented in detail, the calculated GT strength distributions are discussed, and the paper concludes with a summary of the main findings.

2. Theoretical framework

In this work, two main approaches are employed within the QRPA framework: the schematic model (SM) and the Pyatov method (PM). For clarity in presentation, the SM results obtained for the spherical configuration are labeled "SM-sph", while the deformed SM-based calculations are denoted "SM-def". The PM, on the other hand, is restricted to spherical ^{74}Kr (labeled "PM-sph") since its standard formulation does not permit deformation. All models consider nucleons moving in a mean-field potential that includes pairing correlations, while spin–isospin and charge-exchange effects are incorporated through residual interactions within the QRPA framework. In all calculations, the underlying single-particle basis and quasiparticle energies are consistently generated from a phenomenological Woods–Saxon mean field including central, spin–orbit, and Coulomb terms.

2.1. Schematic model (SM)

In SM, the Hamiltonian that governs GT excitations is formulated within the quasiparticle representation as follows:

$$H_{\mathrm{SM}} = H_{\mathrm{sqp}} + h_{ph} + h_{pp}\,, \tag{1}$$

where H_{sqp} represents the single-quasiparticle (sqp) Hamiltonian, while h_{ph} and h_{pp} correspond to the effective interactions in the particle–hole and particle–particle GT channels, respectively [25, 26]. H_{sqp} denotes the single-quasiparticle Hamiltonian, which is written as

$$H_{\mathrm{sqp}} = \sum_{s,\tau,\rho} E_s(\tau)\, \alpha^{\dagger}_{s\rho}\, \alpha_{s\rho}\,, \qquad \tau = n, p\,, \tag{2}$$

where $E_s(\tau)$ stands for the quasiparticle energy of nucleons, while $\alpha^{\dagger}_{s\rho}$ and $\alpha_{s\rho}$ are the corresponding creation and annihilation operators. Here, the index s labels the single-particle state, while ρ denotes the signature (or spin projection) quantum number.

The residual Gamow–Teller interactions acting in the particle–hole (ph) and particle–particle (pp) channels are given by

$$\begin{aligned} h_{ph} &= 2\chi_{ph} \sum_{\mu} \beta^{+}_{\mu} \beta^{-}_{\mu} \,, \\ h_{pp} &= -2\kappa_{pp} \sum_{\mu} P^{+}_{\mu} P^{-}_{\mu} \,, \qquad \mu = 0, \pm 1 \,. \end{aligned} \tag{3}$$

The transition operators in the quasiparticle basis read

$$\beta^{+}_{\mu} = \sum_{n,p,\rho,\rho'} \langle n\rho | \sigma_{\mu} + (-1)^{\mu} \sigma_{-\mu} | p\rho' \rangle \, a^{\dagger}_{n\rho} \, a_{p\rho'} \,, \qquad \beta^{-}_{\mu} = \left(\beta^{+}_{\mu}\right)^{\dagger} \,, \tag{4}$$

$$P^{+}_{\mu} = \sum_{n,p,\rho,\rho'} \langle n\rho | \sigma_{\mu} + (-1)^{\mu} \sigma_{-\mu} | p\rho' \rangle \, a^{\dagger}_{n\rho} \, a^{\dagger}_{p\rho'} \,, \qquad P^{-}_{\mu} = \left(P^{+}_{\mu}\right)^{\dagger} \,. \tag{5}$$

Within the quasiparticle representation, these operators can be recast as

$$\begin{aligned} \beta^{+}_{\mu} &= \sum_{n,p} \left[\frac{1}{\sqrt{2}} \left(\bar{d}_{np} D^{\dagger}_{np} + d_{np} D_{np} \right) + \left(\bar{b}_{np} C^{\dagger}_{np} - b_{np} C_{np} \right) \right] \,, \\ P^{+}_{\mu} &= \sum_{n,p} \left[\frac{1}{\sqrt{2}} \left(b_{np} D^{\dagger}_{np} - \bar{b}_{np} D_{np} \right) + \left(d_{np} C^{\dagger}_{np} + \bar{d}_{np} C_{np} \right) \right] \,, \end{aligned} \tag{6}$$

where D_{np} represents the quasiparticle scattering operator, while $C^{\dagger}_{np}$ and C_{np} are the creation and annihilation operators of neutron–proton two-quasiparticle pairs. According to the quasi-boson approximation, the following commutation relations hold:

$$\left[C_{np}, C^{\dagger}_{n'p'} \right] \approx \delta_{nn'} \delta_{pp'} \,, \qquad \left[C_{np}, C_{n'p'} \right] = 0 \,. \tag{7}$$

Consequently, the effective GT interactions in the quasiparticle space are decomposed as

$$h^{\mathrm{GT}}_{ph} = h^{CC}_{ph} + h^{DD}_{ph} + h^{CD}_{ph} \,, \qquad h^{\mathrm{GT}}_{pp} = h^{CC}_{pp} + h^{DD}_{pp} + h^{CD}_{pp} \,, \tag{8}$$

as detailed in [25].

2.2. Pyatov method (PM)

In the present work, the nuclear mean field entering the quasiparticle Hamiltonian is generated using a phenomenological Woods–Saxon potential, including central, spin–orbit, and Coulomb terms. The inclusion of the spin–orbit interaction leads to a breaking of the spin–isospin SU(4) symmetry underlying the Gamow–Teller operator, which is only approximately preserved at the mean-field level. The strengths of the residual interactions are calibrated by reproducing the experimental position of the Gamow–Teller resonance (GTR). To partially restore the broken spin–isospin SU(4) symmetry, the Pyatov method introduces an additional correction term h_0, which is defined as

$$h_0 = \sum_{\rho=\pm} \frac{1}{2\gamma_\rho} \sum_{\mu=0,\pm1} \Big[\Big[H_{\rm sqp} - (V_c + V_{ls} + V_1), G^{\rho}_{1\mu} \Big]^{\dagger}, \Big[H_{\rm sqp} - (V_c + V_{ls} + V_1), G^{\rho}_{1\mu} \Big] \Big], \tag{9}$$

where γ_ρ is the strength parameter determined by enforcing the commutation relation

$$\gamma_\rho = \frac{\rho}{2} \langle 0 | \Big[\Big[H_{\rm sqp} - (V_c + V_{ls} + V_1), G^{\rho}_{1\mu} \Big], G^{\rho}_{1\mu} \Big] | 0 \rangle . \tag{10}$$

This expression follows the standard Pyatov prescription and is equivalent to the double-commutator form used in earlier works, differing only in notation. The GT transition operator is given by

$$G^{\pm}_{1\mu} = \frac{1}{2} \sum_{k=1}^{A} \left[\sigma_{1\mu}(k) t_+(k) + \rho(-1)^{\mu} \sigma_{1-\mu}(k) t_-(k) \right] , \tag{11}$$

where $\sigma_{1\mu}(k)$ is the spherical component of the Pauli spin operator, and $t_\pm$ are the isospin raising/lowering operators. The PM Hamiltonian, which includes the symmetry-restoring h_0 term, is written as

$$H_{\rm PM} = H_{\rm sqp} + h_0 + h_{ph} + h_{pp} . \tag{12}$$

GT transition strengths are calculated via

$$B^{(\pm)}_{\rm GT}(\omega_i) = \sum_{i,\mu} \left| \langle 1^+_{i,\mu} | G^{\pm}_{1\mu} | 0^+ \rangle \right|^2 , \tag{13}$$

$$B({\rm GT})_\pm = \sum_i B^{(\pm)}_{\rm GT}(\omega_i) , \tag{14}$$

and are constrained by the Ikeda Sum Rule [27], which provides a fundamental benchmark for the consistency of the Gamow–Teller transition calculations

$$\mathrm{ISR} = B(\mathrm{GT}_-) - B(\mathrm{GT}_+) \approx 3(N - Z) . \tag{15}$$

2.3. Pairing and deformation parameters

Pairing gap parameters Δ_n and Δ_p are phenomenologically determined using five-point mass formulas [28]

$$\begin{aligned}\Delta_n \;=\; & \frac{1}{8}[BE(N-2,Z) - 4BE(N-1,Z) + 6BE(N,Z) \\ & -4BE(N+1,Z) + BE(N+2,Z)]\,, \end{aligned} \tag{16}$$

with a similar expression used for Δ_p. For ^{74}Kr, both Δ_n and Δ_p are taken as 1.5 MeV.

The quadrupole deformation parameter β_2 was extracted from the experimental values of the first 2^+ excitation energies [29]. In cases where these data were unavailable, β_2 was deduced from the intrinsic electric quadrupole moment Q_2 (in $e \cdot \mathrm{fm}^2$) through the relation

$$\beta_2 = \frac{4\pi}{3ZR_0^2}\frac{Q_2}{e}\,, \qquad R_0 = 1.2\,A^{1/3}\ \mathrm{fm}\,. \tag{17}$$

For convenience, this expression can also be written in the form

$$\beta_2 = \frac{125\,Q_2}{1.44\,Z\,A^{2/3}}\,, \tag{18}$$

when the quadrupole moment Q_2 is expressed in barns. The β-decay Q-values used in the present study were taken from the AME2020 atomic mass evaluation [30].

3. GT strength distributions

In this section, the Gamow–Teller (GT) strength distributions in ^{74}Kr are investigated within the proton–neutron quasiparticle random-phase approximation (*pn*–QRPA) framework by explicitly considering the effects of nuclear deformation as well as residual interactions. The calculations are performed within this framework using the schematic model (SM), applied to both spherical (SM-sph) and deformed (SM-def) configurations. The underlying single-particle basis and quasiparticle energies are generated from a phenomenological Woods–Saxon mean field including central, spin–orbit, and Coulomb terms. For deformed configurations, axial deformation is introduced through the quadrupole parameter β_2 in the mean-field potential. The particle–hole and particle–particle Gamow–Teller interactions are included in separable form through the standard schematic *pn*–QRPA residual terms h_{ph} and h_{pp} (Section 2), allowing for a systematic investigation of their individual and combined impact on the GT response.

As a consequence of this phenomenological mean-field treatment, the spin–isospin symmetries associated with the Gamow–Teller operator are not fully preserved. Within this framework, the Pyatov method is employed in the spherical limit (PM-sph) to partially restore the broken spin–isospin SU(4)-like symmetry through an additional restoration term. The choice of a Woods–Saxon mean field can influence the fragmentation pattern and centroid energies of the GT strength distributions, particularly at low excitation energies.

For comparison and to place the present results in the context of previous studies, the calculated GT strength distributions are also confronted with the Skyrme–Hartree–Fock plus RPA/TDA results based on the SG2 and SK3 interactions reported by Sarriguren *et al.* [7, 31, 32]. In those calculations, both the single-particle spectrum and the residual interaction are derived self-consistently from the Skyrme energy density functional. Consequently, differences observed between the present SM/PM results and the Skyrme-based calculations reflect not only deformation effects, but also the distinct treatment of residual interactions and ground-state correlations inherent to the two approaches.

The pairing gap parameters (Δ_n, Δ_p) and quadrupole deformation parameters (β_2) adopted in the present calculations are summarized in Table 1. Within the *pn*–QRPA framework based on the schematic model (SM), both spherical and deformed nuclear shapes are considered. The spherical calculations are denoted SM-sph, while the deformed calculations are labeled SM-def. For each deformation type, two distinct equilibrium configurations are obtained. In the oblate case, these configurations are denoted *a* and *b*, whereas for the prolate solutions they are labeled *c* and *d* (*e.g.* oblate^a *versus* oblate^b and prolate^c *versus* prolate^d), as listed in Table 1.

Table 1. Pairing gap parameters for neutrons and protons (Δ_n, Δ_p in MeV) and quadrupole deformation parameters (β_2) adopted in the *pn*–QRPA calculations based on the schematic model (SM).

Configuration		Δ_n	Δ_p	β_2
SM-def	oblate^a	1.5	1.5	−0.15
	oblate^b	1.5	1.5	−0.26
	prolate^c	1.5	1.5	0.25
	prolate^d	1.5	1.5	0.39

3.1. The role of deformation

The nuclear deformation plays a decisive role in shaping the Gamow–Teller (GT) strength distributions, as it modifies the underlying single-particle spectrum and the mixing of nuclear configurations. Therefore, before analyzing the effects of the residual interaction in detail, it is essential to investigate how different deformation scenarios influence the GT response of ^{74}Kr. In the present work, deformation effects are explored by adopting quadrupole deformation parameters from Sarriguren *et al.* [7], namely $\beta_2 = -0.15$ and -0.26 for the oblate shapes and $\beta_2 = 0.39$ for the prolate configuration. In addition, an alternative prolate solution with $\beta_2 = 0.25$, extracted from experimental electric quadrupole moments [33, 34] and evaluated using Eq. (18), is also considered. These configurations are labeled oblate^a, oblate^b, prolate^c, and prolate^d, in accordance with Table 1.

For a meaningful comparison of deformation effects, the particle–hole residual interaction strength in the Gamow–Teller channel was fixed using the standard parametrization $\chi_{ph} = 27/A$ MeV [7], which yields $\chi_{ph} \approx 0.37$ MeV for ^{74}Kr. Throughout the present analysis, the particle–particle interaction strength was fixed to $\kappa_{pp} = 0$, following the earlier *pn*–QRPA studies in this mass region [32]. This parameter set was consistently employed in all calculations. No quenching factor was applied, since the primary objective here is to isolate and examine the intrinsic impact of nuclear deformation on the GT strength distributions without introducing additional renormalization effects. This approach allows for a direct and transparent assessment of deformation-induced modifications and facilitates a clear comparison with earlier theoretical investigations.

It should be noted that, in the GT strength distribution figures, identical vertical scales are not adopted in all panels. This choice is deliberate and aims to preserve the visibility of physically relevant features such as fragmentation patterns, low-energy strength, and deformation-dependent trends. The predicted GT strengths span more than one order of magnitude between different models and configurations; enforcing a common scale would obscure weaker but physically meaningful transitions. Therefore, model-dependent vertical scales are used to ensure clarity and physical interpretability.

In Fig. 1, the calculated Gamow–Teller (GT) strength distributions for ^{74}Kr are compared with the experimental data of Poirier *et al.* [21] to assess the impact of nuclear deformation. The first column displays the measured GT strengths, while the subsequent columns show the results obtained with the single-quasiparticle (sqp) approach, the deformed schematic model calculations (SM-def), and the spherical schematic model together with the Pyatov method (SM-sph and PM-sph). For the sqp and SM-def calculations, both oblate ($\beta_2 < 0$) and prolate ($\beta_2 > 0$) solutions are presented,

whereas the SM-sph and PM-sph results correspond to the spherical configuration. A clear systematic trend is observed: introducing deformation shifts the GT strength distributions toward lower excitation energies and enhances the fragmentation of the total strength. In particular, at $\beta_2 = -0.26$, the SM-def calculations reproduce the experimental peak positions more accurately. The sqp model tends to overestimate the B(GT) amplitudes, whereas the PM-sph results underestimate them. Furthermore, the main resonance peak in the prolate configuration appears at lower energies compared to the oblate case, indicating stronger collectivity in the elongated shape. Overall, the largest discrepancies arise between the oblate and prolate solutions, highlighting the pronounced sensitivity of GT transitions in ^{74}Kr to nuclear shape effects.

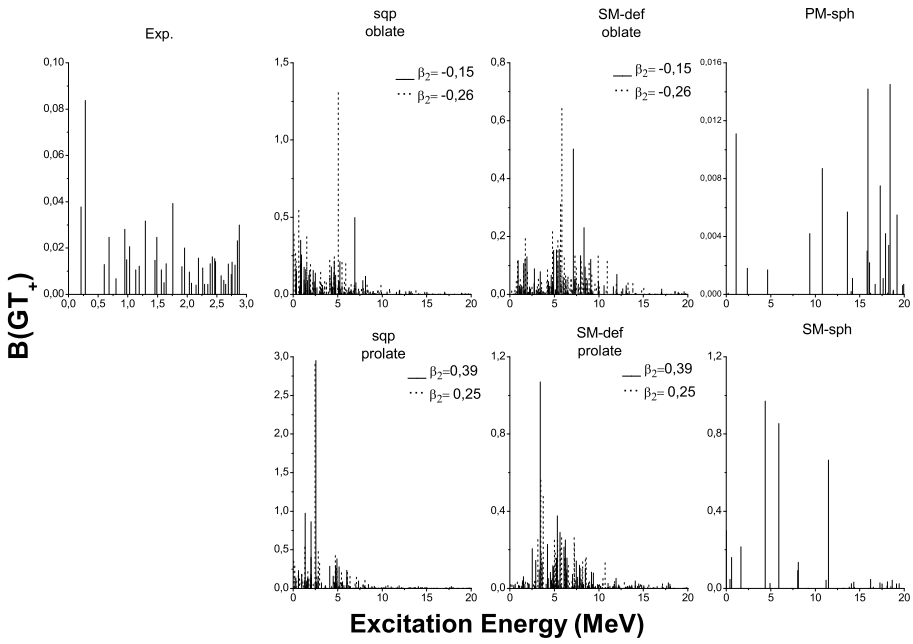

Fig. 1. Comparison of the Gamow–Teller strength distributions $[g_A^2/4\pi]$ in the deformed (oblate and prolate) and spherical configurations of ^{74}Kr with experimental data [21].

The Skyrme–HF-based results of Sarriguren *et al.* are presented in Refs. [7, 31, 32] mainly as the continuous (Gaussian-folded) Gamow–Teller (GT) strength distributions, whereas the present *pn*–QRPA calculations naturally yield discrete transition strengths. Accordingly, the Sarriguren results are shown in the figures as continuous curves, consistent with the original publications, while our results are displayed as discrete spectra (vertical bars),

since applying an additional Gaussian folding to the *pn*–QRPA results would lead to a significant overlap of the many discrete transitions — particularly at low- and intermediate-excitation energies — and obscure the underlying physical information. As the *pn*–QRPA framework is designed to analyze individual transition strengths and their fragmentation explicitly, no additional folding is applied. No numerical transformation between the folded and discrete representations has been performed; the comparison is therefore qualitative, focusing on global features such as fragmentation patterns, centroid shifts, and deformation and residual-interaction effects.

In figures 2–3, the *pn*–QRPA results obtained within the schematic model for deformed shapes (SM-def) are compared with the Gamow–Teller strength distributions reported by Sarriguren *et al.* using the 2qp, TDA, and RPA approaches based on the SG2 Skyrme interaction [7] for the oblate^a ($\beta_2 = -0.15$) and prolate^d ($\beta_2 = 0.39$) configurations of ^{74}Kr. The experimental data from Poirier *et al.* [21] are displayed in the first column of each figure.

In Fig. 2, the second column shows the GT strengths calculated within the Skyrme–Hartree–Fock plus RPA framework using the SG2 interaction, together with the corresponding two-quasiparticle (2qp) results for both the oblate and prolate shapes, while the third column presents the results ob-

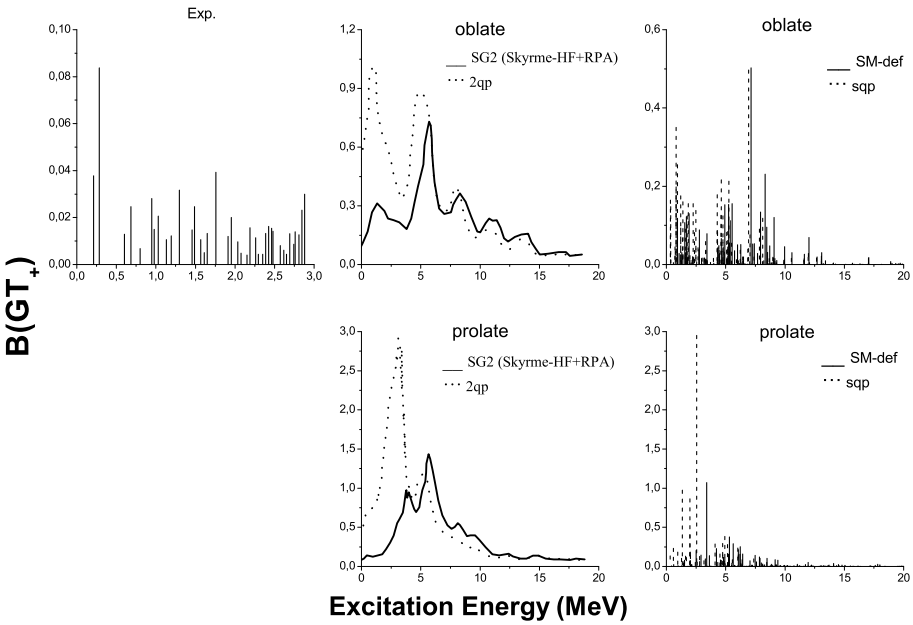

Fig. 2. Comparison of the Gamow–Teller strength distributions $[g_A^2/4\pi]$ obtained from the SG2-based Skyrme–Hartree–Fock + RPA calculations of Sarriguren *et al.* [7] and experimental data [21] for the oblate^a and prolate^d configurations of ^{74}Kr.

tained within the schematic model for the deformed configurations (SM-def), together with the single-quasiparticle (sqp) calculations of the present work. Figure 3 follows the same layout, with the second column representing the TDA results and the third column displaying the SM-def predictions. The experimental GT strengths are confined to the 0–3 MeV excitation-energy region, whereas all theoretical models distribute the strength up to $\sim$ 20 MeV. The SM-def results exhibit stronger fragmentation compared to the other approaches, reflecting enhanced configuration mixing. In the prolate configuration of ^{74}Kr, the 2qp and sqp calculations yield comparable B(GT) values, whereas the Pyatov method applied in the spherical limit (PM-sph) systematically underestimates the strength. The GT 1^+ states obtained within the SM-def calculations are predominantly concentrated in the 0–10 MeV energy range, with the low-energy part (0–3 MeV) being reasonably reproduced by both the SM-def and the SG2-based RPA calculations. Among the models presented in Ref. [7], the SG2 results show the closest agreement with the SM-def strength distributions obtained in the present work.

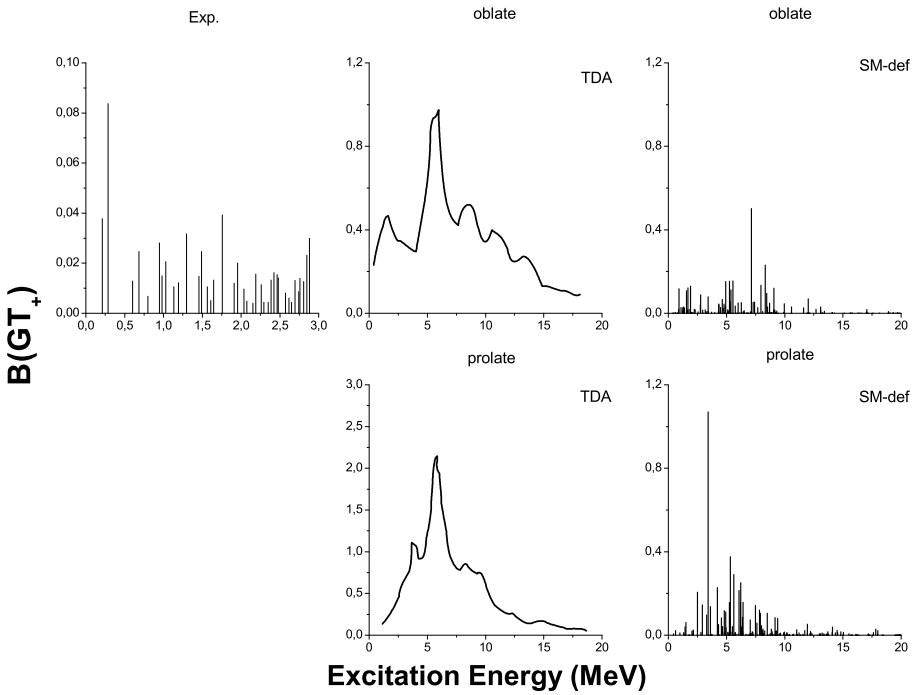

Fig. 3. Comparison of the Gamow–Teller strength distributions $[g_A^2/4\pi]$ obtained from the SG2-based TDA calculations [7] and experimental data [21] for the oblate^a and prolate^d configurations of ^{74}Kr.

The SK3-based RPA strengths [7] displayed in Fig. 4 show a much weaker sensitivity to deformation compared to the SM-def results, whereas the SM-def distributions clearly reflect the difference between the oblate^b ($\beta_2 = -0.26$) and prolate^d configurations. This distinction is particularly important, since in Figs. 2 and 3, the oblate^a configuration is used, while in Fig. 4, the comparison is performed for the oblate^b solution. Moreover, in Figs. 2 and 3, the main GT peak obtained with the SM-def, TDA, and SG2-based RPA calculations increases significantly in amplitude for the prolate configuration compared to the oblate one, while the peak energy remains approximately unchanged and part of the strength is shifted to slightly lower excitation energies in the SM-def results.

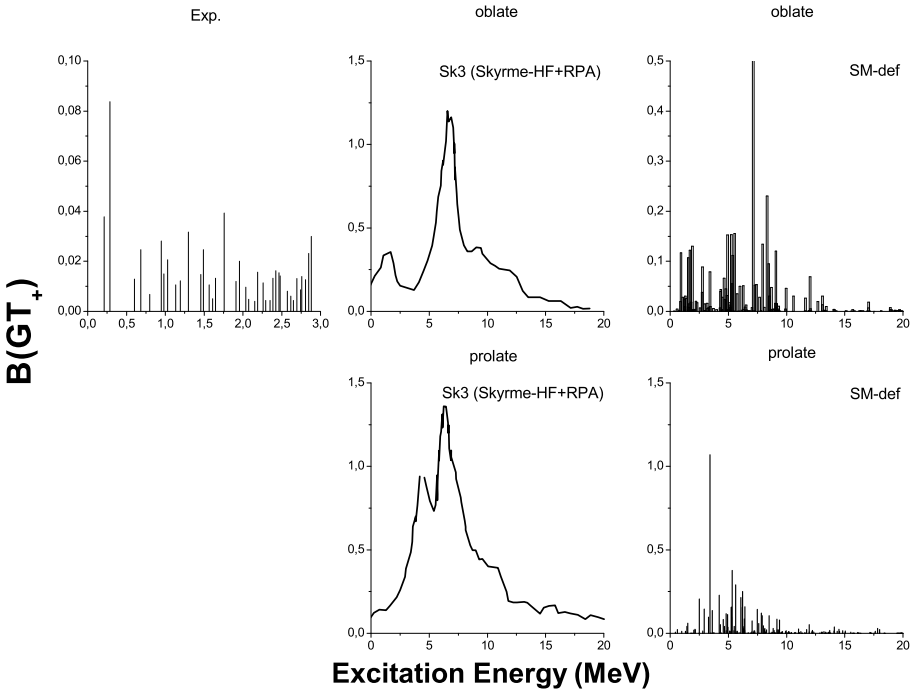

Fig. 4. Comparison of the Gamow–Teller strength distributions [$g_A^2/4\pi$] obtained from the SK3-based RPA calculations [7] and experimental data [21] for the oblate^b and prolate^d configurations of ^{74}Kr.

3.2. The role of residual interactions

The residual interaction parameters χ_{ph} and κ_{pp} significantly affect the GT strength distributions. Several values have been used in the literature depending on the mass region [35–39]. In the present *pn*–QRPA calculations, the standard schematic-model parametrization $\chi_{ph} = 27/A \approx 0.37$ MeV

for ^{74}Kr is adopted in both the spherical and deformed SM calculations, while the same value is used as the baseline choice in the spherical PM framework [7, 32]. The particle–particle interaction strength κ_{pp} is varied from 0 to 0.07 MeV [32].

Figures 5 and 6 illustrate the influence of the residual interactions on the GT response within the schematic model (SM) and the Pyatov method (PM). In Fig. 5, the first two columns correspond to the oblate configuration (left: SG2, right: SM-def), whereas the last two columns represent the prolate configuration (left: SG2, right: SM-def), all calculated for the same set of the κ_{pp} values. A clear and systematic trend is observed: increasing the *pp* interaction strength shifts the GT strength toward lower excitation energies and reduces the total strength at higher energies. This attractive interaction enhances fragmentation, leading to an increased number of peaks in the SM-def spectra. The position of the dominant GT resonance shows only a minor shift in energy, while its intensity decreases with increasing κ_{pp}, particularly in the prolate configuration. At low excitation energies ($E <$ 5 MeV), a slight enhancement of the GT strength is also observed, indicating that the *pp* channel plays a non-negligible role in feeding low-lying 1^+ states.

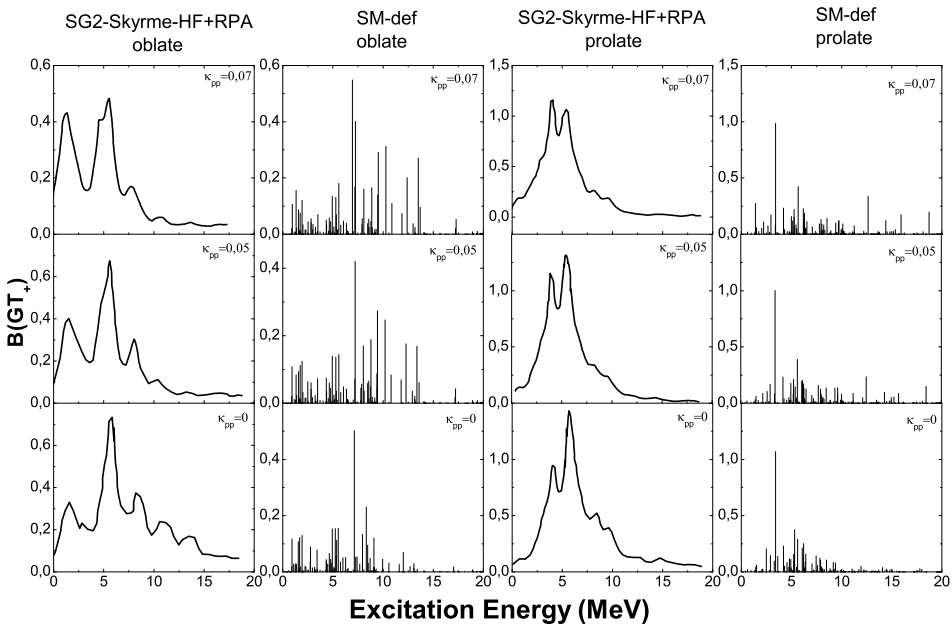

Fig. 5. Comparison of the Gamow–Teller strength distributions $[g_A^2/4\pi]$ obtained from the SG2-based RPA [32] and SM-def calculations for the oblate^a and prolate^d configurations of ^{74}Kr. The calculations are performed for different values of the particle–particle coupling strength κ_{pp}.

Figure 6 further examines the effect of the *pp* interaction for spherical ^{74}Kr using the Pyatov method (PM-sph) and the schematic model (SM-sph). In the PM-sph calculations (left column), increasing κ_{pp} leads to a pronounced downward shift of the GT strength toward lower excitation energies together with a strong redistribution of the strength. In particular, in the absence of *pp* correlations ($\kappa_{pp} = 0$), the inclusion of the symmetry-restoring term h_0 in the PM framework results in a drastic reduction of the dominant GT peaks, with the maximum strength decreasing by about two orders of magnitude compared to the corresponding SM-sph case. This strong quenching reflects the restoration of spin–isospin SU(4)-like symmetry in the ground state, which is explicitly violated at the mean-field level. The Pyatov method effectively removes spurious collectivity associated with symmetry breaking, leading to a more fragmented and less collective GT response. In contrast, the SM-sph results (right column), where no symmetry restoration is applied, exhibit a qualitatively different behavior: the inclusion of the *pp* force suppresses the total strength more moderately, without the

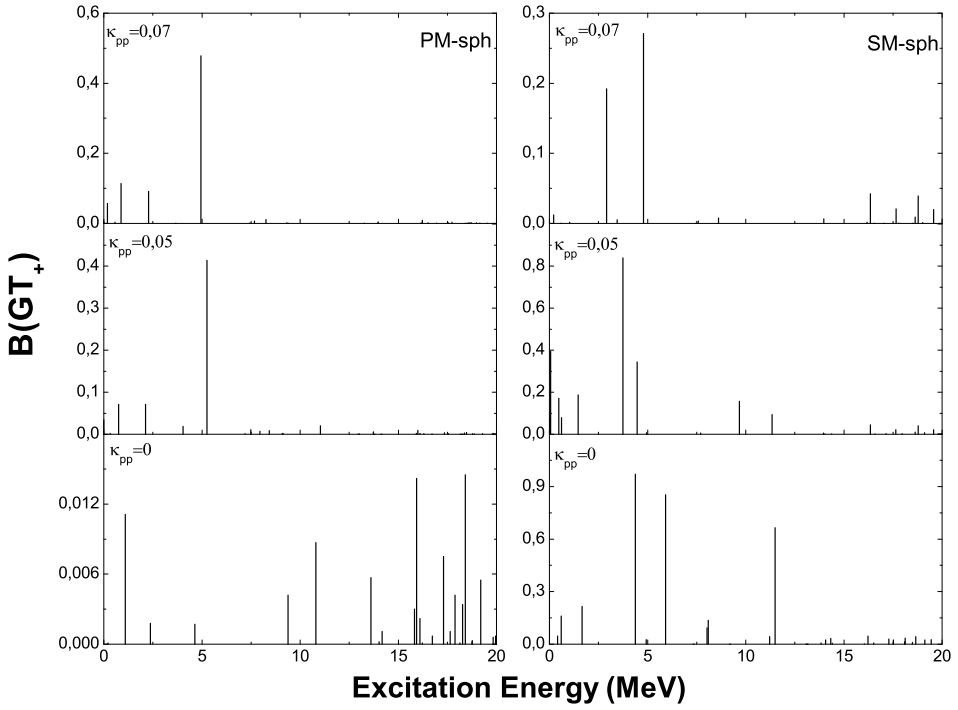

Fig. 6. Comparison of the Gamow–Teller strength distributions $[g_A^2/4\pi]$ for the spherical ^{74}Kr obtained using the SM-sph and PM-sph approaches. The calculations are performed for different values of the particle–particle coupling strength κ_{pp}.

dramatic redistribution observed in the PM calculations. This contrasting behavior demonstrates that the *pp* interaction plays a more collective and symmetry-driven role within the PM scheme, while in the SM approach, its effect remains largely perturbative. Similar sensitivity of GT strengths to symmetry restoration within the Pyatov framework has been reported in the earlier studies of neutron-deficient nuclei, confirming that this behavior is a general feature of the method rather than a peculiarity of ^{74}Kr.

It should be noted that two slightly different χ_{ph} choices are used in this section for different purposes. In Figs. 5–6, we adopt the standard schematic-model parametrization $\chi_{ph} = 27/A \approx 0.37$ MeV for ^{74}Kr to establish the baseline sensitivity to κ_{pp}. In Figs. 7–9, χ_{ph} is fixed to 0.48 MeV in order to reproduce the parameter set employed in Ref. [31] for a direct, one-to-one (like-for-like) comparison. For consistency with Ref. [31], the particle–particle interaction strength was kept at $\kappa_{pp} = 0$, and the same deformation parameters were adopted, namely $\beta_2 = -0.15$ for the oblate shape and $\beta_2 = 0.39$ for the prolate configuration.

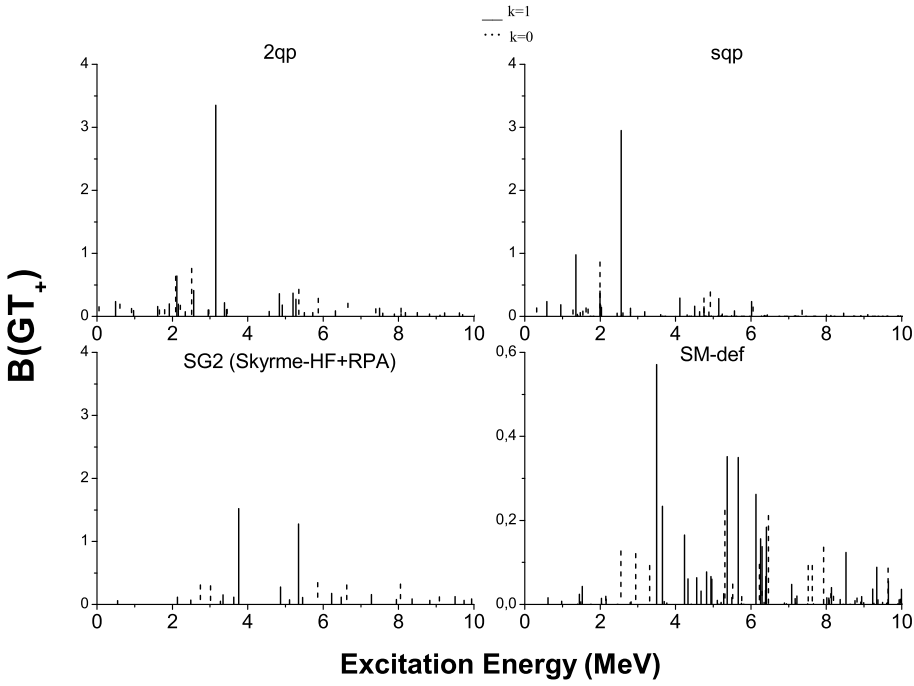

Fig. 7. Comparison of the Gamow–Teller strength distributions $[g_A^2/4\pi]$ for the prolate^d configuration of ^{74}Kr obtained from the SG2-based RPA [31] and SM-def calculations. The panels display the $k = 0$ (dashed vertical lines) and $k = 1$ (solid vertical lines) excitation modes.

In Fig. 7, the GT strength distributions for the prolate shape are shown separately for $k = 0$ and $k = 1$ excitations in the 0–10 MeV region. This separation is necessary in deformed systems, since the GT strength splits into $k = 0$ and $k = 1$ components, corresponding to the projection of the total angular momentum on the symmetry axis. Although allowed GT transitions do not change parity, the partition of strength between the $k = 0$ and $k = 1$ branches is governed by the deformation-dependent Nilsson structure and the corresponding QRPA configuration mixing, and may therefore differ between oblate and prolate shapes. The GT strengths obtained with the SM-def and sqp models are compared with the two-quasiparticle (2qp) and Skyrme–Hartree–Fock + RPA (SG2) results of Ref. [31]. Both models reproduce the experimental low-energy strength reasonably well, although the SM-def calculation exhibits stronger fragmentation for both k components.

Figure 8 illustrates the effect of varying the ph residual interaction strength in deformed ^{74}Kr. For both the oblate and prolate shapes, the SG2-based RPA [31] and the SM-def results are displayed side by side for $\chi_{ph} = \chi/2$, χ, and 2χ. Two systematic effects of the repulsive ph channel are clearly visible:

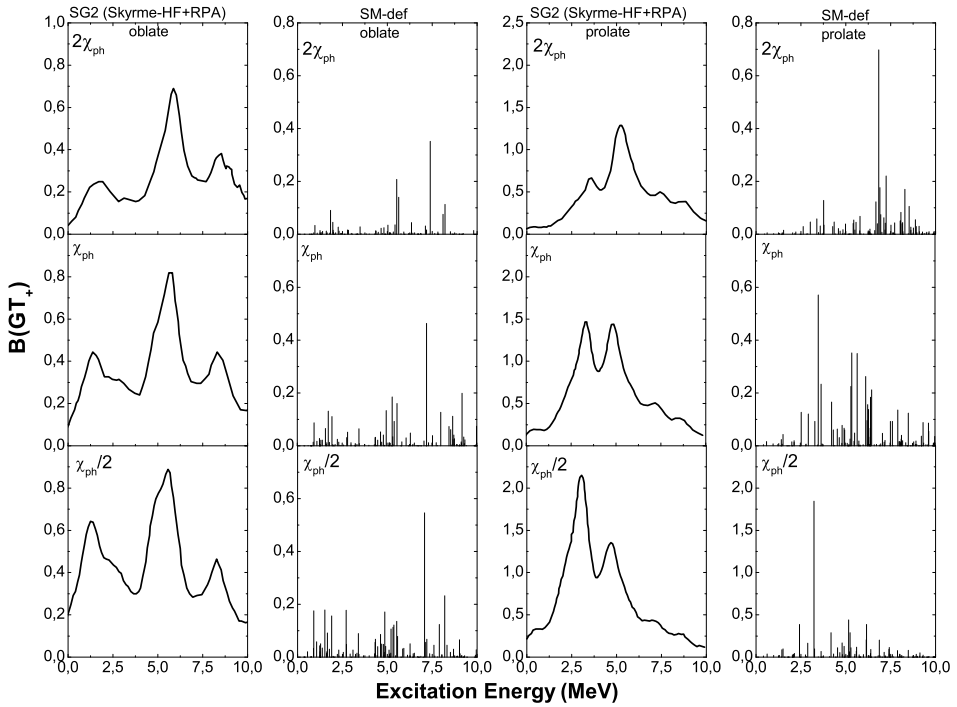

Fig. 8. Comparison of the Gamow–Teller strength distributions for the oblate[a] and prolate[d] configurations of ^{74}Kr obtained from the SG2-based RPA [31] and SM-def calculations for different values of the particle–hole coupling strength χ_{ph}.

(i) it shifts the GT strength toward higher excitation energies, displacing the main resonance peak; and *(ii)* it reduces the total strength, particularly above 5 MeV. These effects become progressively more pronounced with increasing χ_{ph}.

The corresponding behavior in the spherical limit is analyzed in Fig. 9, where the SG2-based RPA [31], SM-sph, and PM-sph results are shown in the first, second, and third columns, respectively. In all three models, increasing χ_{ph} leads to a suppression of the total B(GT) strength. However, while the SM-sph and SG2-based RPA calculations shift the main 1^+ peak to higher energies, the PM-sph results exhibit a more moderate energy displacement but a stronger overall suppression at low energies. This comparison highlights the different treatments of ground-state correlations in these models and reveals that the *ph* interaction acts predominantly as a quenching mechanism in the spherical ^{74}Kr.

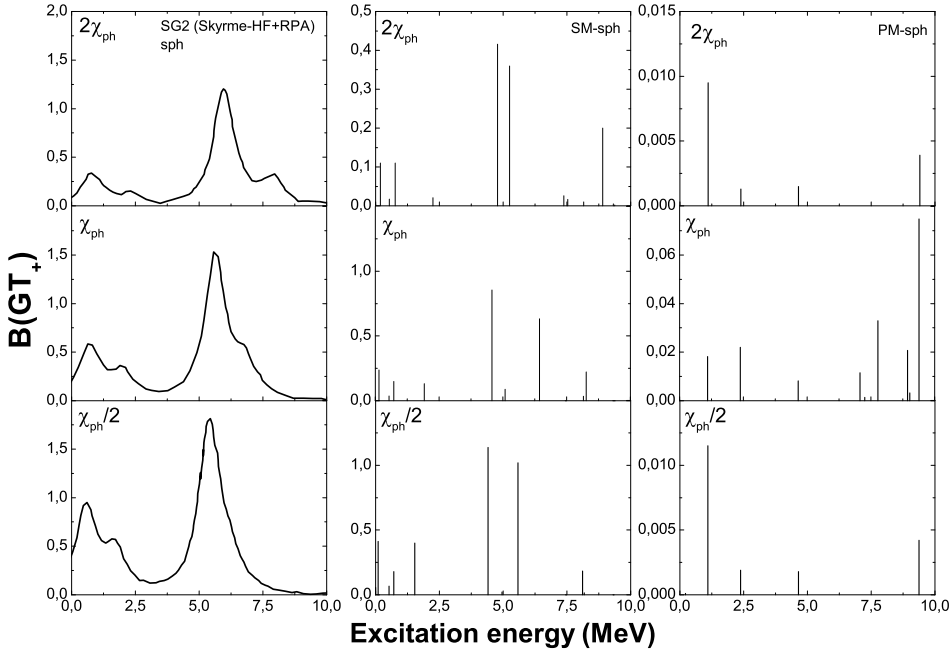

Fig. 9. Comparison of the Gamow–Teller strength distributions for the spherical ^{74}Kr obtained from the SG2-based RPA [31], SM-sph, and PM-sph calculations for different values of the particle–hole coupling strength χ_{ph}.

3.3. Ikeda sum rule and energy-weighted summed strength

The Gamow–Teller strengths are expected to obey the Ikeda Sum Rule (ISR),

$$\mathrm{ISR} = \sum B(\mathrm{GT}_-) - \sum B(\mathrm{GT}_+) \approx 3(N-Z)\,,$$

which provides a stringent model-independent constraint on the GT response.

Table 2 lists the integrated $\sum B(\mathrm{GT}_-)$ and $\sum B(\mathrm{GT}_+)$ values up to $E_{\mathrm{cut}} = 30$ MeV for all models considered. The values corresponding to the $k = 0$ component are given explicitly, while the $k = 1$ contributions are shown in parentheses. All models reproduce the ISR within a few percent accuracy, indicating that the SM-def, SM-sph, and PM-sph frameworks conserve the GT sum rule without requiring renormalization of g_A.

Table 2. Results from the SM-def, SM-sph, and PM-sph calculations corresponding to the oblate, prolate, and spherical shapes in ^{74}Kr are presented. The third and fourth columns show the GT strength, expressed in units of $[g_A^2/4\pi]$, for the β^- and β^+ decay summed up to a cutoff energy of $E_{\mathrm{cut}} = 30$ MeV. The fifth column provides the Ikeda sum rule for this energy cutoff, and the final column displays the energy-weighted summed strength in units of $[\mathrm{MeV}g_A^2/4\pi]$ corresponding to the β^+ decay. All results are presented for $k = 0$ and $k = 1$ (the latter in parentheses). Additionally, the results from SG2-based RPA and TDA calculations [7] are also included.

Models		$\sum B(\mathrm{GT}_-)$	$\sum B(\mathrm{GT}_+)$	ISR	$\sum EB(\mathrm{GT}_+)$
SG2 (Skyrme-HF+RPA)	oblate[a]	3.880(7.228)	1.886(3.239)	5.984	12.65(23.76)
	prolate[d]	4.431(9.758)	2.437(5.769)	5.983	17.31(36.86)
SG2 (Skyrme-HF+TDA)	oblate[a]	4.517(8.305)	2.523(4.315)	5.984	16.95(31.22)
	prolate[d]	5.294(11.952)	3.300(7.964)	5.983	23.56(52.32)
SM-def	oblate[a]	3.257(6.232)	1.397(2.466)	5.626	17.70(18.84)
	oblate[b]	3.433(7.016)	1.602(3.362)	5.485	17.68(14.23)
	prolate[c]	3.486(8.101)	1.882(4.374)	5.331	12.36(12.69)
	prolate[d]	3.839(8.322)	1.953(4.579)	5.629	12.97(11.79)
PM-sph	spherical	5.898	0.125	5.774	37.11
SM-sph	spherical	10.085	4.371	5.714	50.96

The last column of Table 2 reports the energy-weighted summed strengths, again separated into $k = 0$ and $k = 1$ components. A systematic reduction of the energy-weighted sum is observed when the spherical configuration is deformed. This decrease suggests that deformation redistributes the GT strength over a broader excitation range, thereby quenching the collective

low-energy response. This behavior is consistent with the enhanced fragmentation observed in the SM-def results, confirming that deformation softens the GT response even when the total ISR strength is preserved.

3.4. Total half-life and log(ft) values

The calculation of β^+-decay half-lives is an important benchmark for testing the reliability of Gamow–Teller strength distributions. In this work, half-lives are evaluated using

$$(ft)_{\beta^\mp} = \frac{D}{(g_A/g_V)^2 4\pi B_{\mathrm{GT}}(I_i \to I_f, \beta^\mp)} \tag{19}$$

with $D = 6295$ s and $(g_A/g_V) = -1.254$ [40]. No quenching of the axial coupling was applied. The phase-space factors (Fermi integrals) $f(Z, Q_{EC} - \omega_i)$ were evaluated according to the standard expressions and tabulations given in Refs. [41, 42], using the experimental Q_{EC} values from AME2020 to define the maximum lepton energy and the decay window for each transition.

In the calculation of the total half-lives and $\log(ft)$ values, the particle–hole and particle–particle residual interaction strengths were fixed to $\chi_{ph} = 0.37$ and $\kappa_{pp} = 0$, respectively, in all SM and PM calculations. Table 3 presents a comparison of the GT transition energies and $\log(ft)$ values obtained from the SM-sph, SM-def, and PM-sph calculations with experimental data [43, 44]. The SM-sph results reproduce the experimental $\log(ft)$ values most closely, with the PM-sph calculations giving slightly larger deviations, while the SM-def predictions exhibit a stronger sensitivity to nuclear deformation; however, this deformation effect does not manifest as a uniform increase or decrease in $\log(ft)$ but rather varies depending on the specific transition and on whether the $k = 0$ or $k = 1$ component dominates.

The corresponding β^+-decay half-lives are summarized in Table 4. The experimental half-life of ^{74}Kr is 11.5 minutes [28, 45]. The PM-sph and SM-sph models reproduce this value most accurately, predicting 10.81 min and 10.33 min, respectively. In contrast, the SM-def predictions exhibit a stronger shape dependence, ranging from 7.65 to 16.76 min depending on the oblate or prolate configuration. When compared with the earlier SG2-based RPA and TDA results from Ref. [7], the present SM-sph and PM-sph models demonstrate improved agreement with experiment, particularly for spherical and near-spherical configurations. It should be emphasized that the improved agreement with experimental data obtained within the spherical SM-sph and PM-sph calculations does not imply that nuclear deformation plays a minor role in the description of the GT response of ^{74}Kr. On the contrary, the present results clearly demonstrate that deformation strongly affects the fragmentation pattern and energy distribution of the GT strength.

Table 3. The GT transition energies and log(ft) values for the ^{74}Kr isotope are calculated using the schematic model (SM) and the Pyatov method (PM). For PM, only spherical (s) results are reported, whereas for SM both the spherical (s) and the deformed prolate configuration (p^c) with $\beta_2 = 0.25$ are considered. In the latter case, the deformed ^{74}Kr results are given separately for $k = 0$ and $k = 1$. $^{74}_{36}$Kr$(0^+, \text{g.s.}) \rightarrow {}^{74}_{35}Br(1^+)Q(\text{g.s.}) = 2.975$ MeV.

SM		PM		SM-def				Exp.		
s		s		p^c ($k = 0$)		p^c ($k = 1$)				
ω [MeV]	log(ft)	ω [MeV]	log(ft)	ω [MeV]	log(ft)	ω [MeV]	log(ft)	ω [MeV]	I %	log(ft)
0	4.13	0	8.84	0.437	5.31	0.614	4.82	0.212	31	4.8
0.411	4.92	0.223	7.85	1.302	5.09	0.981	5.10	0.306	41	4.6
0.597	4.39	1.098	5.55	1.565	9.39	1.402	6.25	0.609	3.1	5.4
1.658	4.29	2.38	6.35	1.659	7.89	1.442	4.56	0.701	3.2	5.3
				1.835	6.33	1.481	5.46	0.970	1	5.5
				2.03	7.92	1.521	4.39			
				2.129	4.78	1.738	7.09			
				2.508	3.86	1.812	7.83			
				2.916	4.01	2.025	5.95			
						2.028	4.88			
						2.151	4.86			
						2.448	6.53			
						2.790	5.01			
						2.802	5.96			

The improvement observed in the PM framework reflects the impact of restoring spin–isospin symmetry broken at the mean-field level, which is a physical effect distinct from nuclear deformation. These two mechanisms act at different levels and should be regarded as complementary. A simultaneous treatment of deformation and symmetry restoration within the same theoretical framework could further modify the results, an issue that is beyond the scope of the present study and deserves future investigation.

For a meaningful comparison with the results of Sarriguren *et al.*, special care has been taken to adopt the same set of fundamental constants whenever possible. In the present calculations, the standard value $D = 6295$ s and the unquenched axial-vector coupling constant were used, in accordance with Refs. [7, 31, 32]. Furthermore, the same deformation parameters and residual interaction strengths were employed. Unlike the Skyrme-based calculations of Refs. [7, 31, 32], the Q_{EC} values in the present work were not derived self-consistently from the mean-field single-particle and quasiparticle energies. Instead, the experimental Q_{EC} values taken from the AME2020 atomic mass evaluation were used solely to define the decay window and the phase-space factors entering the Fermi integrals. The β^+-decay half-lives

Table 4. Results of total half-lives ($T_{1/2}$) of ^{74}Kr from the SM-def, SM-sph, and PM-sph calculations corresponding to the oblate, prolate, and spherical shapes. Additionally, the results from RPA and TDA with SG2 forces [7] are also included. The comparison of the half-life values obtained from theoretical models with the experimentally determined values [28, 45] is presented.

Models		$T_{1/2}$
Exp.		11.5 m
SG2 (Skyrme-HF+RPA)	oblate[a]	10.0 m
	prolate[d]	14.0 m
SG2 (Skyrme-HF+TDA)	oblate[a]	7.4 m
	prolate[d]	10.4 m
SM-def	oblate[a]	7.65 m
	oblate[b]	8.86 m
	prolate[c]	10.99 m
	prolate[d]	16.76 m
PM-sph	spherical	10.81 m
SM-sph	spherical	10.33 m

were then obtained within the standard ft formalism by combining these phase-space factors with the *pn*–QRPA Gamow–Teller strength distributions. Therefore, the comparison presented here reflects differences arising primarily from the underlying theoretical frameworks and the treatment of deformation and residual interactions, rather than from different choices of Q_{EC} values.

These findings indicate that symmetry-restoring terms, together with an appropriate treatment of nuclear deformation, are essential ingredients for reliable β-decay rate predictions in neutron-deficient nuclei.

4. Conclusion

The β^+-decay characteristics and the Gamow–Teller (GT) strength distributions of ^{74}Kr are of particular importance for modeling weak-interaction processes in astrophysical environments such as supernovae and X-ray bursts. The accurate GT strengths directly influence nucleosynthesis pathways and the thermal evolution of stellar matter.

The SM-def calculations exhibit a significantly stronger fragmentation of the GT strength compared to the spherical SM-sph and PM-sph results, reflecting the well-known impact of nuclear deformation on the redistribution

of Gamow–Teller strength. This enhanced fragmentation is in closer qualitative agreement with experimentally observed spreading patterns, although it does not necessarily imply a uniformly improved quantitative reproduction of integrated observables such as half-lives or $\log(ft)$ values. Nuclear deformation generally shifts the GT strength toward lower excitation energies and increases its spreading, particularly for the prolate configuration with $\beta_2 = 0.25$.

The inclusion of particle–particle (pp) and particle–hole (ph) residual interactions introduces competing effects on the GT distributions. The attractive pp interaction lowers the GT strength and redistributes it toward lower excitation energies, while the repulsive ph interaction shifts the main resonances to higher energies and reduces their overall magnitude. In addition, the symmetry-restoring term h_0 employed in the PM-sph calculations leads to a marked improvement in the agreement with experimental $\log(ft)$ values by compensating for broken symmetries inherent in the mean-field approximation.

A key outcome of the present work is that the calculated half-lives and $\log(ft)$ values — especially those obtained within the SM-sph and PM-sph frameworks — reproduce the available experimental data without the need for any quenching of the axial-vector coupling constant. This indicates that the adopted models effectively account for the dominant nuclear correlations and do not rely on additional empirical renormalization of g_A, thereby enhancing their predictive reliability.

All calculated GT strength distributions satisfy the Ikeda sum rule to a high degree of accuracy, confirming the internal consistency of the employed frameworks. The analysis of energy-weighted summed strengths further highlights the role of deformation in redistributing transition strength over a wider excitation-energy range.

In summary, although several decay studies of ^{74}Kr have been reported in the literature, the present work is based on the proton–neutron QRPA framework and employs the schematic model and the Pyatov method built on a Woods–Saxon mean field. This approach differs conceptually from the self-consistent Skyrme–Hartree–Fock-based QRPA calculations. Within this context, nuclear deformation effects are explicitly investigated through the SM-def calculations, while the spherical SM-sph and PM-sph results serve as benchmark cases to disentangle deformation effects from symmetry-restoration effects. The calculated half-lives and $\log(ft)$ values reproduce the available experimental data without introducing additional empirical renormalization, such as quenching of the axial-vector coupling constant. The particle–hole and particle–particle residual interactions follow standard prescriptions commonly adopted in pn–QRPA studies and are not tuned on a nucleus-by-nucleus basis beyond the standard pn–QRPA prescriptions.

The present results demonstrate that nuclear deformation and residual interactions play distinct and complementary roles in shaping the Gamow–Teller response of ^{74}Kr. A simultaneous treatment of nuclear deformation and symmetry restoration within a unified framework, particularly for the Pyatov method, is beyond the scope of the present work and will be addressed in future studies.

This work was supported by the Eskisehir Osmangazi University Scientific Research Projects (BAP), Project No. FBA-2025-3578.

REFERENCES

[1] H. Schatz *et al.*, «rp-process nucleosynthesis at extreme temperature and density conditions», *Phys. Rep.* **294**, 167 (1998).

[2] A. Petrovici, K.W. Schmid, A. Faessler, «Beyond mean field approach to the beta decay of medium mass nuclei relevant for nuclear astrophysics», *Prog. Part. Nucl. Phys.* **66**, 287 (2011).

[3] A. Petrovici, K.W. Schmid, A. Faessler, «Neutron–proton pairing correlations in medium mass $N \sim -Z$ nuclei», *Nucl. Phys. A* **647**, 197 (1999).

[4] A. Petrovici, K.W. Schmid, A. Faessler, «Microscopic aspects of shape coexistence in ^{72}Kr and ^{74}Kr», *Nucl. Phys. A* **665**, 333 (2000).

[5] A. Petrovici, K.W. Schmid, A. Faessler, «Variational approach to shape coexistence in ^{82}Se», *Nucl. Phys. A* **710**, 246 (2002).

[6] J.J. Cowan, F.-K. Thielemann, J.W. Truran, «The R-process and nucleochronology», *Phys. Rep.* **208**, 267 (1991).

[7] P. Sarriguren, E. Moya de Guerra, A. Escuderos, «Shapes and β-decay in proton rich Ge, Se, Kr and Sr isotopes», *Nucl. Phys. A* **658**, 13 (1999).

[8] I. Hamamoto, «Neutron–proton interaction and allowed beta-decay of G–T type», *Nucl. Phys.* **62**, 49 (1965).

[9] J. Krumlinde, P. Möller, «Calculation of Gamow–Teller β-strength functions in the rubidium region in the RPA approximation with Nilsson-model wave functions», *Nucl. Phys. A* **417**, 419 (1984).

[10] P. Möller, J. Randrup, «New developments in the calculation of β-strength functions», *Nucl. Phys. A* **514**, 1 (1990).

[11] M. Hirsch, A. Staudt, K. Muto, H.V. Klapdor-Kleingrothaus, «Microscopic calculation of β^+EC decay half-lives with atomic numbers $Z = 10$–30», *Nucl. Phys. A* **535**, 62 (1991); K. Muto, E. Bender, H.V. Klapdor, «Proton–neutron quasiparticle RPA and charge-changing transitions», *Z. Phys. A* **333**, 125 (1989); H. Homma *et al.*, «Systematic study of nuclear β decay», *Phys. Rev. C* **54**, 2972 (1996).

[12] F. Frisk, I. Hamamoto, X.Z. Zhang, «Gamow–Teller β^+ decay of deformed nuclei near the proton drip line», *Phys. Rev. C* **52**, 2468 (1995).

[13] I. Hamamoto, X.Z. Zhang, «Dependence of Gamow–Teller β^+-decay of ^{80}Zr, ^{76}Sr and ^{72}Kr on nuclear shape», *Z. Phys. A* **353**, 145 (1995).

[14] N.I. Pyatov, D. Salamov, «Conservation laws and collective excitations in nuclei», *Nucleonica* **22**, 127 (1977).

[15] O. Civitarese, P.D. Hess, J.G. Hirsch, M. Reboiro, «Spontaneous and dynamical breaking of mean field symmetries in the proton–neutron quasi particle random phase approximation and the description of double β decay transitions», *Phys. Rev. C* **59**, 194 (1998).

[16] A.A. Kulliev *et al.*, «Rotational Invariant Model of the States with $K^\pi = 1^+$ and Their Contribution to the Scissors Mode», *Int. J. Mod. Phys. E* **9**, 249 (2000).

[17] N. Cakmak, «The study of Charge Exchange collective Excitations in Odd mass nuclei», Ph.D. Thesis, 2008.

[18] T. Babacan, D.I. Salamov, A. Kucukbursa, «The effect of the pairing interaction on the energies of isobar analog resonances in $^{110-124}$Sb and isospin admixture in Sn isotopes», *J. Phys. G: Nucl. Part. Phys.* **30**, 759 (2004).

[19] T. Babacan, D.I. Salamov, A. Kucukbursa, «Gamow–Teller 1^+ states in ^{208}Bi», *Phys. Rev. C* **71**, 037303 (2005).

[20] T. Babacan, D.I. Salamov, A. Kucukbursa, «The Investigation of the $\log(ft)$ Values for the Allowed Gamow–Teller Transitions of Some Deformed Nuclei», *Math. Comput. Appl.* **10**, 359 (2005).

[21] E. Poirier *et al.*, «B(GT) strength from β-decay measurements and inferred shape mixing in ^{74}Kr», *Phys. Rev. C* **69**, 034307 (2004).

[22] C. Chandler *et al.*, «Evidence for a highly deformed oblate 0^+ state in $^{74}_{36}$Kr», *Phys. Rev. C* **56**, R2924 (1997).

[23] A. Petrovici, K.W. Schmid, A. Faessler, «Shape coexistence and shape transition in $N \simeq Z$ nuclei from krypton to molybdenum», *Nucl. Phys. A* **605**, 290 (1996).

[24] A. Petrovici *et al.*, «Shape coexistence phenomena in medium mass nuclei», *Prog. Part. Nucl. Phys.* **43**, 485 (1999).

[25] S. Cakmak, J.-U. Nabi, T. Babacan, C. Selam, «Study of Gamow–Teller transitions in isotopes of titanium within the quasi particle random phase approximation», *Astrophys. Space Sci.* **352**, 645 (2014).

[26] N. Cakmak, S. Unlu, C. Selam, «Gamow–Teller 1^+ states in $^{112-124}$Sb isotopes», *Pramana — J. Phys.* **75**, 649 (2010).

[27] K.I. Ikeda, «Collective Excitation of Unlike Pair States in Heavier Nuclei», *Prog. Theor. Phys.* **31**, 434 (1964).

[28] G. Audi, A.H. Wapstra, «The 1995 update to the atomic mass evaluation», *Nucl. Phys. A* **595**, 409 (1995).

[29] S. Raman *et al.*, «Transition probability, $B(E2)\uparrow$, from the ground to the first-excited 2^+ state of even–even nuclides», *At. Data Nucl. Data Tables* **36**, 1 (1987).

[30] M. Wang *et al.*, «The AME2020 atomic mass evaluation (II). Tables, graphs and references», *Chinese Phys. C* **45**, 030003 (2021).

[31] P. Sarriguren, E. Moya de Guerra, A. Escuderos, A.C. Carrizo, «β decay and shape isomerism in ^{74}Kr», *Nucl. Phys. A* **635**, 55 (1998).

[32] P. Sarriguren, E. Moya de Guerra, A. Escuderos, «β decay in odd-A and even–even proton-rich Kr isotopes», *Phys. Rev. C* **64**, 064306 (2001).

[33] P. Möller, J.R. Nix, «Atomic masses and nuclear ground-state deformations calculated with a new macroscopic–microscopic model», *At. Data Nucl. Data Tables* **26**, 165 (1981).

[34] P. Möller *et al.*, «Nuclear Ground-State Masses and Deformations», *At. Data Nucl. Data Tables* **59**, 185 (1995).

[35] C. Gaarde *et al.*, «Collective isospin-spin excitations and Gamow–Teller strength», in: «Proceedings of the 4$^{\text{th}}$ International Conference on Nuclei Far from Stability», Helsingør, Denmark, 7–13 June, 1981, pp. 281–286.

[36] E. Bender, K. Muto, H.V. Klapdor, «Calculation of β^--decay half-lives with the proton–neutron quasiparticle RPA», *Phys. Lett. B* **208**, 53 (1988).

[37] S.P. Ivanova, A.A. Kuliev, D.I. Salamov, «Strength Functions of β-decay of $^{117-123}$Ba isotopes», *Sov. J. Nucl. Phys.* **24**, 278 (1976).

[38] S.P. Ivanova, A.A. Kuliev, D.I. Salamov, «1^+ collective states of ^{124}Cs and ^{126}Cs nuclei», *Izv. Akad. Nauk SSSR, Ser. Fiz.* **41**, 131 (1977).

[39] H. Homma *et al.*, «Systematic study of nuclear β decay», *Phys. Rev. C* **54**, 2972 (1996).

[40] E.K. Warburton, I.S. Towner, B.A. Brown, «First-forbidden β decay: Meson-exchange enhancement of the axial charge at $A \sim 16$», *Phys. Rev. C* **49**, 824 (1994).

[41] J. Suhonen, «From Nucleons to Nucleus: Concepts of Microscopic Nuclear Theory», *Springer*, Berlin 2007.

[42] Surender, V. Kumar, P.C. Srivastava, «Study of β^+/EC-decay properties of *sd* shell nuclei using nuclear shell model», *Ann. Phys.* **470**, 169772 (2024).

[43] F.G. Kondev *et al.*, «The NUBASE2020 evaluation of nuclear physics properties», *Chinese Phys. C* **45**, 030001 (2021).

[44] National Nuclear Data Center (NNDC), NuDat 2.8 database, `https://www.nndc.bnl.gov/nudat2/`

[45] G. Audi, O. Bersillon, J. Blachot, A.H. Wapstra, «The NUBASE evaluation of nuclear and decay properties», *Nucl. Phys. A* **624**, 1 (1997).